

NOTICE IN COMPLIANCE WITH PUBLISHER POLICY: An edited version of this paper was published by AGU. Copyright © 2005 American Geophysical Union. Available at: <http://dx.doi.org/10.1029/2004WR003239>

Comparison of two-dimensional and three-dimensional simulations of dense nonaqueous phase liquids (DNAPLs): Migration and entrapment in a nonuniform permeability field

John A. Christ

Environmental and Water Resources Engineering Program, University of Michigan, Ann Arbor, Michigan, USA

Lawrence D. Lemke

Environmental Sciences Program, Department of Geology, Wayne State University, Detroit, Michigan, USA

Linda M. Abriola

Department of Civil and Environmental Engineering, Tufts University, Medford, Massachusetts, USA

Received 5 April 2004; revised 19 August 2004; accepted 4 October 2004; published 14 January 2005.

[1] The influence of reduced dimensionality (two-dimensional (2-D) versus 3-D) on predictions of dense nonaqueous phase liquid (DNAPL) infiltration and entrapment in statistically homogeneous, nonuniform permeability fields was investigated using the University of Texas Chemical Compositional Simulator (UTCHEM), a 3-D numerical multiphase simulator. Hysteretic capillary pressure–saturation and relative permeability relationships implemented in UTCHEM were benchmarked against those of another lab-tested simulator, the Michigan-Vertical and Lateral Organic Redistribution (M-VALOR). Simulation of a tetrachloroethene spill in 16 field-scale aquifer realizations generated DNAPL saturation distributions with approximately equivalent distribution metrics in two and three dimensions, with 2-D simulations generally resulting in slightly higher maximum saturations and increased vertical spreading. Variability in 2-D and 3-D distribution metrics across the set of realizations was shown to be correlated at a significance level of 95–99%. Neither spill volume nor release rate appeared to affect these conclusions. Variability in the permeability field did affect spreading metrics by increasing the horizontal spreading in 3-D more than in 2-D in more heterogeneous media simulations. The assumption of isotropic horizontal spatial statistics resulted, on average, in symmetric 3-D saturation distribution metrics in the horizontal directions. The practical implication of this study is that for statistically homogeneous, nonuniform aquifers, 2-D simulations of saturation distributions are good approximations to those obtained in 3-D. However, additional work will be needed to explore the influence of dimensionality on simulated DNAPL dissolution.

Citation: Christ, J. A., L. D. Lemke, and L. M. Abriola (2005), Comparison of two-dimensional and three-dimensional simulations of dense nonaqueous phase liquids (DNAPLs): Migration and entrapment in a nonuniform permeability field, *Water Resour. Res.*, 41, W01007, doi:10.1029/2004WR003239.

1. Introduction

[2] The migration and entrapment of dense nonaqueous phase liquids (DNAPLs) at the field scale is poorly understood. Systematic field experiments are generally prohibited, accidental spills are difficult to characterize [e.g., Pouslen and Kueper, 1992; Kueper et al., 1993; Essaid et al., 1993], and field-scale heterogeneity is rarely recreated in the lab [Kueper et al., 1993; Kueper and Gerhard, 1995; Imhoff et al., 2003]. Consequently, numerical models have become the primary method for the investigation and characterization of field-scale DNAPL migration and entrapment [Essaid and Hess, 1993; Kueper and Gerhard, 1995; Dekker and Abriola, 2000; Lemke et al., 2004a].

[3] Over the last two decades a number of numerical models capable of simulating the migration of DNAPL through porous media have been developed. These models range in complexity from one-dimensional, single-component, two-phase models to three-dimensional, multi-component, multiphase (up to 4) flow models with dynamic partitioning between phases (for a review, see Abriola [1989], Miller et al. [1998], and Adeel et al. [2001]). These models have typically been used to simulate hydrophobic contaminant (e.g., tetrachloroethene (PCE)) migration in two-dimensional (2-D) flow fields [Kueper and Frind, 1991; Essaid and Hess, 1993; Essaid et al., 1993; Brown et al., 1994; Kueper and Gerhard, 1995; Bradford et al., 1998; Dekker and Abriola, 2000; Whittaker et al., 2000; Lemke and Abriola, 2003; Lemke et al., 2004a], with relatively few studies undertaking 3-D simulations. Implicit in the use of 2-D simulations is the assumption that DNAPL

migration is relatively unaffected by the nominal 2-D domain width and porous media property variability in the third dimension. Given this assumption, 2-D saturation distributions, as characterized by quantitative metrics (e.g., center of mass, organic spreading, maximum saturation, etc.), are thought to be good representations of the more realistic 3-D domain. However, to date, the validity of this assumption has not been systematically investigated. If it could be shown that 2-D simulations provide reasonable representations of 3-D saturation distributions, then it would be justifiable to investigate migration and entrapment in the more computationally efficient 2-D domain. Conversely, the identification of consistent differences between saturation distributions simulated in 2-D and 3-D could lead to improved interpretations of 2-D modeling and laboratory results.

[4] Existing modeling studies that have considered the third dimension typically have done so for a single realization and have neglected heterogeneity and/or hysteretic capillary effects [Faust et al., 1989; Brown et al., 1994; Panday et al., 1994; Edwards et al., 1999]. Guarnaccia and Pinder [1998] appear to be the only researchers to consider the effect of reduced model dimensionality on the prediction of the DNAPL distribution. However, they did so for a single homogeneous realization at the lab-scale (1 m × 1 m × 0.3 m). Thus no study has systematically investigated the effect of dimensionality on the simulated infiltration and entrapment of DNAPL in field-scale nonuniform porous media.

[5] The purpose of this work is to investigate the effect of reduced dimensionality on simulated DNAPL saturation distributions using a suite of three-dimensional, statistically homogeneous, nonuniform permeability fields that are representative of a natural formation. DNAPL saturation distribution metrics are used to quantitatively compare predictions of DNAPL entrapment in two and three dimensions. Variations in contaminant recovery predictions due to reduced dimensionality (2-D versus 3-D) will be investigated in a subsequent paper.

2. Methods

[6] Numerical simulations were performed in two and three dimensions using a version of the University of Texas Chemical Compositional Simulator (UTCHEM 9.0) [Delshad et al., 1996], modified to simulate hysteretic infiltration and entrapment in nonuniform permeability fields. UTCHEM has been used to simulate a number of 2-D and 3-D physicochemical source zone remediation scenarios (e.g., Surfactant Enhanced Aquifer Remediation (SEAR)) [Brown et al., 1994; Edwards et al., 1999; University of Texas Chemical Compositional Simulator (UTCHEM), 2000; Wu et al., 2000; Delshad et al., 2000; Roeder and Falta, 2001; Ouyang et al., 2002] and partitioning tracer tests [Jin et al., 1997; Young et al., 1999]. Its application to model hysteretic DNAPL infiltration and entrapment, however, has not been documented in the literature. To provide validation for this application, 2-D DNAPL simulations generated using UTCHEM were benchmarked against simulations generated with the Michigan-Vertical and Lateral Organic Redistribution (M-VALOR) simulator [Rathfelder and Abriola, 1998]. M-VALOR is a multiphase flow code that has been used extensively to simulate 2-D, two-phase immiscible con-

taminant transport in lab and field-scale heterogeneous subsurface systems [Demond et al., 1996; Dekker and Abriola, 2000; Rathfelder et al., 2000; Drummond et al., 2000; Rathfelder et al., 2003; Lemke and Abriola, 2003]. Comparisons between 2-D saturation profiles generated with both models using identical input parameters led to the discovery of coding errors in the entrapment subroutine in UTCHEM. After modification of this subroutine to correctly simulate the two-phase capillary pressure – saturation – relative permeability relationship with entrapment, 2-D saturation distributions simulated using both models were essentially identical (maximum absolute difference in maximum organic saturation <2%), demonstrating that the modified version of UTCHEM was functioning properly.

[7] UTCHEM solves a mass conservation equation in terms of the overall volume of component κ per unit pore volume (\tilde{C}_κ) [Delshad et al., 1996]:

$$\frac{\partial}{\partial t} (n\tilde{C}_\kappa\rho_\kappa) = \nabla \cdot \left[\sum_{\alpha=1}^{n_p} \rho_\kappa \left(C_\kappa^\alpha \frac{kk_{r\alpha}}{\mu_\alpha} \cdot (\nabla P^\alpha - \rho^\alpha g \nabla h) - n_{s_\alpha} D_\kappa^\alpha \cdot \nabla C_\kappa^\alpha \right) \right] + R_\kappa, \quad (1)$$

where

$$\tilde{C}_\kappa = (1 - \hat{C}_\kappa) \sum_{\alpha=1}^{n_p} s_\alpha C_\kappa^\alpha + \hat{C}_\kappa. \quad (2)$$

In equations (1) and (2), α denotes the fluid phase ($\alpha = w, o$ for water and organic phases, respectively), n is the matrix porosity, k is the intrinsic permeability, ρ^α is the α fluid density, ρ_κ is the κ component density, μ_α is the α fluid viscosity, P^α is the α fluid phase pressure, s_α is the saturation of the α phase, $k_{r\alpha}$ is the relative permeability to the α fluid, D_κ^α is the dispersion tensor, C_κ^α is the concentration of component κ in phase α , \hat{C}_κ is the sorbed concentration of component κ , R_κ is a source/sink term, g is the gravitational vector, h is depth, n_p is the number of phases, and t is time. Development of (1) assumes slightly compressible porous media and fluids and accounts for mass transfer across phase boundaries. The problem considered in this work involves immiscible flow of a pure DNAPL. Thus $C_\kappa^\alpha = 0$ or 1, $\hat{C}_\kappa = 0$, and $\tilde{C}_\kappa = s_w$ or s_o . Equation (1) is constrained by the conservation relationship $s_w + s_o = 1$. UTCHEM solves these volumetric concentration equations on a uniform block-centered finite difference grid using an implicit pressure, explicit saturation (IMPES) type scheme. Several upstream weighting options are available for the advection term. In this work first-order upstream weighting was selected to facilitate the comparisons with M-VALOR.

[8] To investigate the effect of reduced dimensionality on DNAPL saturation distributions, 21 3-D permeability realizations were selected from a suite of realizations developed by Lemke et al. [2004a]. These realizations are representative of a field-scale formation, whose properties are based on an aquifer located in Oscoda, Michigan, USA. This aquifer underlies a former dry cleaning business and is contaminated with PCE DNAPL. It is composed of relatively homogeneous glacial outwash sands and was the site of a pilot-scale SEAR test designed to remove residual PCE from a known source zone [Abriola et al., 2005]. Realiza-

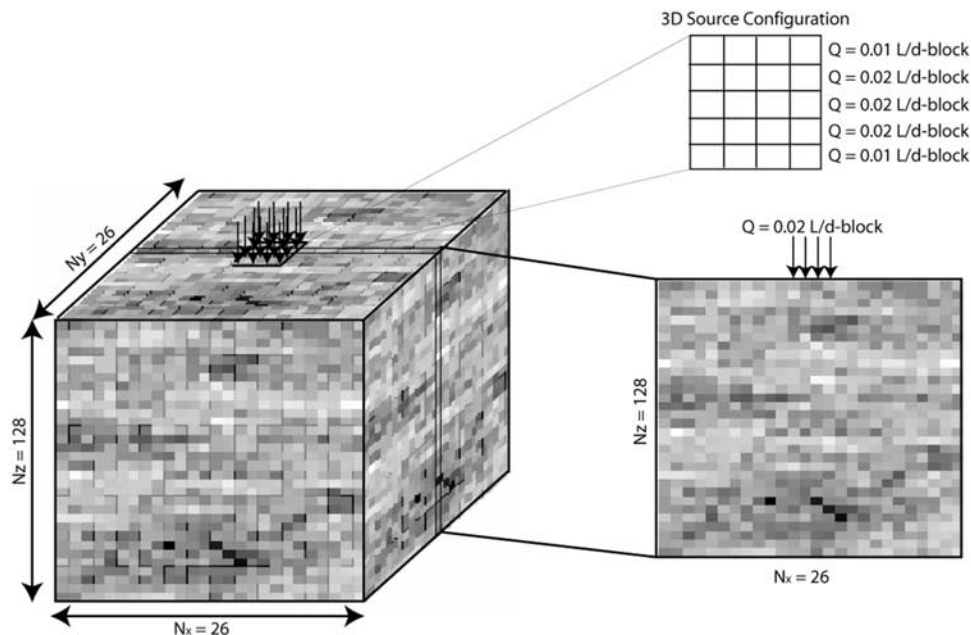


Figure 1. Model domain conceptualization for two-dimensional (2-D) and 3-D simulations. The nominal width of the 2-D domain is equal to the width of the 3-D cross section, and the release rate configuration in 3-D was selected so that the sum of the rows (x direction) was equal to the sum of the columns (y direction).

tion selection criteria were based on DNAPL mass distribution metrics (maximum organic saturation and vertical and lateral spreading) calculated from results of 50 2-D PCE infiltration simulations generated using MVALOR [Lemke *et al.*, 2004a]. Realizations representing minimum, mean, and maximum values for three selected metrics (see below) were chosen to span the range of variability. Four additional realizations with metric values approximately corresponding to the 0.2, 0.4, 0.6, and 0.8 quantiles were selected for each metric. These selection criteria resulted in some duplication of the realizations chosen, so that the number of unique 3-D permeability realizations was actually 16. To facilitate direct comparisons between 2-D and 3-D simulations, the 2-D realizations used in this study were extracted directly from the center x - z cross section of the 3-D simulation (Figure 1), resulting in 16 3-D and 16 2-D permeability realizations. This number of realizations is similar to the number employed for previous DNAPL saturation distribution studies [Dekker and Abriola, 2000; Kueper and Gerhard, 1995].

[9] The selected 3-D modeling domain (7.925 m long (x) by 7.925 m wide (y) by 9.754 m deep (z)) was sized to be consistent with the installed remediation system and was oriented so that the center x - z cross section (henceforth referred to as the center cross section) connected the SEAR extraction well with the center injection well (Figure 1) [Lemke *et al.*, 2004a]. To resolve the influence of capillary property variation at the modeled scale of heterogeneity (30.48 cm), the 3-D domain was discretized into 86,528 cells with 26 cells in the x direction, 26 cells in the y direction, and 128 cells in the z direction. This level of spatial resolution represents a reasonable trade-off between model accuracy and computational demands [Rathfelder and Abriola, 1998; Glass *et al.*, 2000; Lemke *et al.*, 2004a]. The 2-D simulations were conducted for the center

cross section. In both 2-D and 3-D simulations, cell size in the x , y , and z direction was 30.48 cm, 30.48 cm, and 7.62 cm, respectively. In all simulations the upper and lower boundary of the domain were specified as no flow boundaries and the side boundaries were specified as constant pressure and maintained a constant organic saturation equal to zero. The domain size was sufficiently extensive such that no organic phase crossed the lateral boundaries during any simulation. A uniform saturation ($s_w = 1$) corresponding to hydrostatic conditions was specified at time $t = 0$.

[10] Porous media properties of the selected realizations were based on 167 samples collected from vertical and directional cores at the Oscoda site [Drummond *et al.*, 2000; Abriola *et al.*, 2005]. Statistically homogeneous, nonuniform permeability fields were generated using sequential Gaussian simulation (SGS) [Deutsch and Journel, 1998] following the procedure outlined by Lemke *et al.* [2004a]. These efforts utilized a zonal anisotropy model [Journel and Huijbregts, 1978] with a nugget effect and spherical semi-variogram. Variability in the horizontal plane was modeled as isotropic and a uniform vertical to horizontal permeability ratio of 0.5 was assigned to all cells to account for anisotropy due to aquifer stratification at a scale not resolved by the geostatistical methods. A uniform porosity of 0.36 was used in all simulations. As indicated above, resolution of the simulated permeability field was 30.48 cm in the horizontal and vertical directions (1 horizontal by 4 vertical grid blocks). The mean hydraulic conductivity, K , value was 16.8 m/d and the variance of the lognormal transformed K field ($\sigma^2 \ln(K)$) was 0.29 [Lemke *et al.*, 2004a]. Soil properties and variogram parameters are summarized in Table 1.

[11] The P_c - s_{α} - $k_{r\alpha}$ relationship implemented in this work combined the Brooks-Corey [Brooks and Corey, 1964] P_c - s_{α} model with the Burdine [1953] $k_{r\alpha}$ -model integrated

Table 1. Numerical Simulation Input Parameters

| Parameter | Water | PCE |
|---|-------------------------|----------|
| Fluid properties | | |
| Density, g/cm ³ | 0.999032 | 1.625 |
| Viscosity, cP | 1.121 | 0.89 |
| Compressibility, Pa ⁻¹ | 4.4 × 10 ⁻¹⁰ | 0.0 |
| Initial saturation | 1.0 | 0.0 |
| $P_c - s_{\alpha} - k_{r\alpha}$ model parameters | | |
| (Reference) air entry pressure, kPa | 2.809 | |
| Pore size index | 2.0773 | |
| Interfacial tensions | | |
| Air/water, dynes/cm | 72.75 | |
| Oil/water, dynes/cm | 47.8 | |
| Irreducible water saturation | 0.080 | |
| Max residual organic saturation | 0.151 | |
| Matrix properties | | |
| Variogram Parameters | horizontal | vertical |
| Nugget | 0.333 | 0.333 |
| Range, m | 7.0 | 1.07 |
| Integral scale, m | 2.33 | 0.36 |
| Porosity | 0.36 | |
| Reference permeability, μm ² | 19.7 | |
| Domain discretization | | |
| Δx, m | 0.3048 | |
| Δy, m | 0.3048 | |
| Δz, m | 0.0726 | |

into the hysteretic entrapment model developed by *Parker and Lenhard* [1987]. This approach accounts for hysteresis due to organic entrapment by including an apparent water saturation, which is a function of the actual water saturation and the entrapped organic saturation, in the organic phase relative permeability function (see *Rathfelder and Abriola* [1998] for a complete presentation of hysteretic model equations). Model parameters to describe a representative P_c-s_{α} soil moisture characteristic curve were derived from aquifer samples using the method of *Haverkamp and Parlange* [1986] and are given in Table 1. *Leverett* [1941]

scaling was used to scale this reference (ref) P_c-s_{α} curve to k and n in each cell according to the expression

$$P_c = P_c^{ref} \sqrt{\frac{k^{ref}}{k} \frac{n}{n^{ref}}}. \quad (3)$$

In this work, uniform porosity is assumed so that $n = n^{ref}$. [12] A hypothetical DNAPL spill, consistent with the suspected release from the former dry cleaning building, was simulated in the 16 3-D realizations by releasing 128 liters of PCE over a 400 day period in a 4×5 cell area centered in the top layer of the 3-D model. As shown in Figure 1, the release rate in each cell block was selected to approximate a symmetric source by balancing the sum of the release rates in the x and y directions. For 2-D simulations, PCE was released at an equivalent rate (0.02 L/d) in each of the center four cells of the top layer of the center 2-D cross section (Figure 1), corresponding to a total of 32L of PCE released over the 400 day period. In all simulations the 400 day spill event was followed by a 330 day redistribution period (730 day simulation) to allow for organic entrapment.

[13] To quantify the similarities and differences in saturation distributions simulated in 2-D and 3-D, four DNAPL mass distribution metrics were examined: (1) the maximum organic saturation (s_o^{max}), (2) the second spatial moment about the center of mass in the x direction (σ_{xx}^2), (3) the second spatial moment about the center of mass in the z direction (σ_{zz}^2), and (4) the saturation distribution ganglia-to-pool (GTP) mass ratio. Spatial moments are a commonly used metric for quantifying saturation distributions [*Kueper and Frind*, 1991; *Essaid and Hess*, 1993; *Kueper and Gerhard*, 1995; *Lemke et al.*, 2004a] and may be defined as

$$M_{ij} = \int_{-\infty}^{\infty} \int_{-\infty}^{\infty} n \rho^o s_o(x, z) x^i z^j dx dz. \quad (4)$$

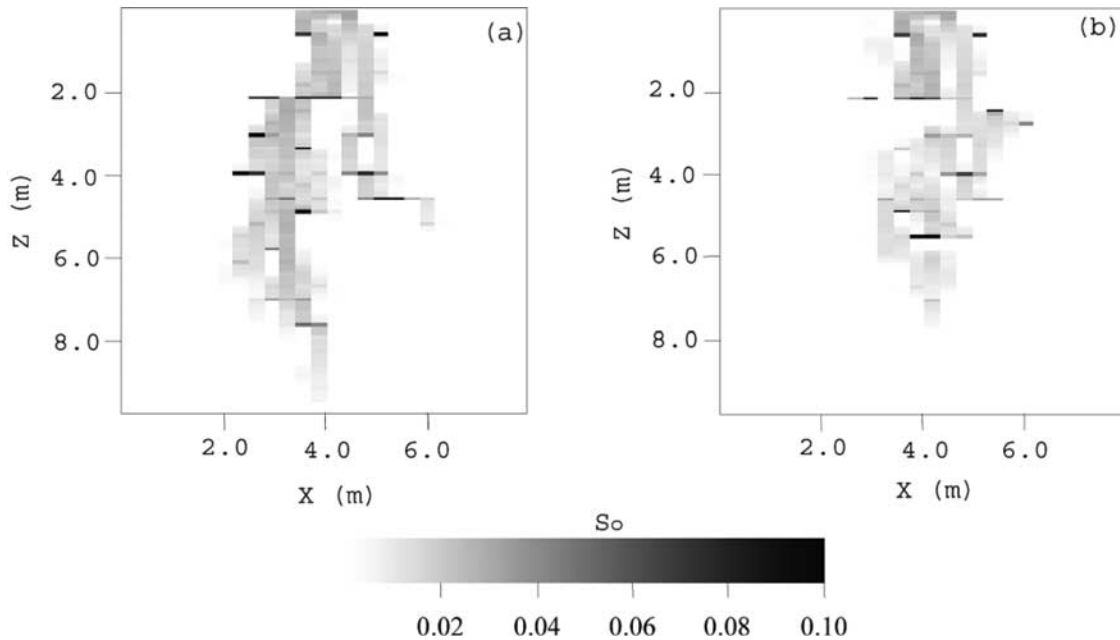


Figure 2. Saturation profiles simulated in (a) 2-D using UTCHEM and in (b) the same 2-D slice extracted from a 3-D UTCHEM simulation.

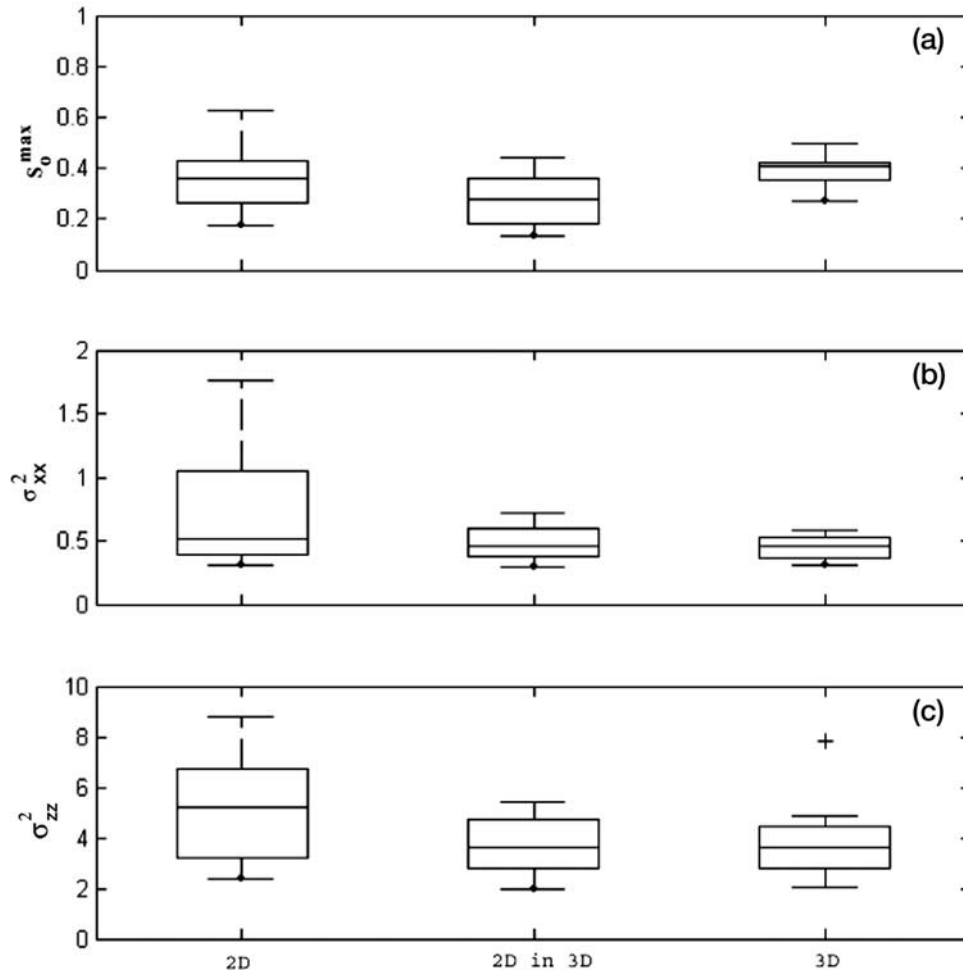


Figure 3. Box plot comparing 2-D, “2-D in 3-D,” and 3-D metric distributions for all 16 permeability realizations: (a) s_o^{\max} , (b) σ_{xx}^2 , and (c) σ_{zz}^2 . The box extends from the $q_{0.25}$ to the $q_{0.75}$ quartile (interquartile range (IQR)) and is separated by the median. The whiskers extend from the box to the minimum and maximum metric value within $1.5 \cdot \text{IQR}$. An asterisk indicates a probable outlier (metric value $>3 \cdot \text{IQR}$).

The second spatial moment about the center of mass is then

$$\sigma_{xx}^2 = \frac{M_{20}}{M_{00}} - X_{cm}^2 \quad \sigma_{zz}^2 = \frac{M_{02}}{M_{00}} - Z_{cm}^2, \quad (5)$$

where

$$X_{cm} = \frac{M_{10}}{M_{00}} \quad Z_{cm} = \frac{M_{01}}{M_{00}} \quad (6)$$

are the center of mass in the horizontal (X_{cm}) and vertical directions (Z_{cm}), respectively. In (4)–(6), x is the horizontal coordinate, z is the vertical coordinate, and i and j are the moment orders. M_{00} , the zeroth moment, is a measure of the organic mass in the domain.

[14] The GTP mass ratio is a metric recently used to quantify the temporal evolution of a source zone [Lemke *et al.*, 2004b] and is defined as the mass of PCE in cells with organic saturations less than the maximum residual organic saturation (ganglia) divided by the mass of PCE in cells with saturations greater than or equal to the maximum residual organic saturation (pools). This mass ratio may be

a better indicator of subsequent dissolution behavior of DNAPL saturation distributions [Lemke *et al.*, 2004b] than X_{cm} or Z_{cm} , which are reported here for completeness.

[15] The metrics above were calculated for the saturation distributions simulated in the 16 selected 3-D permeability realizations and the 16 corresponding 2-D permeability realizations. In addition, 2-D saturation metrics for the center x - z cross section of each 3-D simulation were examined. Statistical tests were then used to determine the extent of similarity between the two- and three-dimensional DNAPL saturation distributions. The realizations were ranked according to their corresponding metric values to investigate migration and entrapment behavior for the ensemble of realizations. The saturation structure of the 3-D simulations was also used to investigate the assumption of statistical isotropy of permeability imposed in the horizontal plane.

[16] Finally, the influence of nonuniformity was further investigated by performing additional simulations in selected realizations with a higher degree of spatial variability. The three realizations that had previously generated the min, mean, and max s_o^{\max} values (a normally distributed

Table 2. Statistics for Saturation Distribution Metrics in Two-Dimensional (2-D) and 3-D Realizations

| Metric | Minimum | Mean | Maximum | Standard Deviation |
|--------------------------------------|---------|--------|----------|--------------------|
| 2-D s_o^{\max} | 0.172 | 0.363 | 0.626 | 0.127 |
| 2-D in 3-D s_o^{\max} ^a | 0.134 | 0.277 | 0.442 | 0.101 |
| 3-D s_o^{\max} ^b | 0.272 | 0.390 | 0.494 | 0.055 |
| 2-D X_{cm} | 3.593 | 4.014 | 5.064 | 0.400 |
| 2-D in 3-D X_{cm} | 3.531 | 3.939 | 4.320 | 0.250 |
| 3-D X_{cm} | 3.671 | 3.943 | 4.339 | 0.166 |
| 2-D σ_{xx}^2 | 0.303 | 0.696 | 1.759 | 0.423 |
| 2-D in 3-D σ_{xx}^2 | 0.291 | 0.480 | 0.717 | 0.142 |
| 3-D σ_{xx}^2 | 0.304 | 0.444 | 0.584 | 0.092 |
| 2-D Z_{cm} | 2.748 | 3.969 | 4.736 | 0.627 |
| 2-D in 3-D Z_{cm} | 2.255 | 3.147 | 3.880 | 0.501 |
| 3-D Z_{cm} | 2.527 | 3.275 | 4.252 | 0.403 |
| 2-D σ_{zz}^2 | 2.403 | 5.176 | 8.777 | 2.031 |
| 2-D in 3-D σ_{zz}^2 | 1.971 | 3.656 | 5.385 | 1.088 |
| 3-D σ_{zz}^2 | 2.018 | 3.790 | 7.797 | 1.372 |
| 2-D GTP | 1.343 | 8.930 | 24.081 | 6.789 |
| 2-D in 3-D GTP ^c | 2.880 | 18.631 | ∞ | 19.081 |
| 3-D GTP | 3.874 | 10.324 | 23.05 | 5.160 |

^aMetrics calculated for center 2-D x - z cross section in 3-D simulation.

^bMetrics calculated for entire 3-D domain.

^cThe one realization that resulted in an infinite GTP mass ratio was ignored for the statistical calculations.

metric) in the center cross section of the 3-D domain were transformed by scaling the permeability field from $\sigma^2 \ln(K) = 0.29$ to $\sigma^2 \ln(K) = 1.0$.

3. Results and Analysis

3.1. Saturation Distribution Comparisons

[17] Comparison of saturation distributions simulated in 2-D with those computed for the center x - z cross section of 3-D simulations illustrate some general similarities and differences that are typically encountered. Figure 2 depicts two representative PCE saturation distributions; one generated in 2-D (2a) and the other in 3-D (2b) using a profile extracted from the same 3-D permeability realization. The 3-D realization has been sliced to reveal the center x - z cross section corresponding to the 2-D domain. Despite the presence of identical permeability fields and release rates in the cross section, the appearance of the saturation distributions generated in 2-D and 3-D is quite different. The saturation distribution in the 3-D model appears more discontinuous, has a higher center of mass, and displays less spreading in the vertical direction. These characteristics are attributed to the movement of PCE out of the plane into adjacent sections and were generally observed in all 16 simulation comparisons. Note, however, that high-saturation cells, indicative of pools, appear at many of the same locations in both the 2-D and 3-D realizations. This observation is important, given the significance of pools in governing the persistence of DNAPL in a source zone [Anderson et al., 1992; Sale and McWhorter, 2001; Lemke et al., 2004b] and the influence pools have on the value of the saturation distribution metrics.

[18] Although the appearance of the saturation distributions simulated in 2-D and 3-D for a single realization can appear quite different (Figure 2), the behavior of the ensemble of realizations must be considered to assess the ability of 2-D simulations to adequately represent 3-D simulations. Ensemble statistics calculated for the saturation

moment metrics described in section 2 are reported in Table 2 for both 2-D simulations and 2-D cross sections extracted from 3-D simulations (2-D in 3-D). The mean spreading metric values calculated in 2-D simulations tend to be approximately 20–30% higher than the metrics derived from “2-D in 3-D” simulations. A paired t-test [Devore, 1995] confirmed that the 2-D simulation metrics are greater than the “2-D in 3-D” simulation metrics at the 98–99% (depending on the metric) confidence level. The variance in spreading metric values for this ensemble of 16 realizations is approximately twice as large in 2-D simulations as it is in 2-D cross sections extracted from 3-D simulations. This variability is better visualized in Figure 3, which compares the distribution of metric values in 2-D and “2-D in 3-D” using box plots. In this figure each box represents the interquartile range and is separated by the median. The vertical lines extend to the minimum and maximum metric values and the points represent outliers as described in the figure caption. For the simulated conditions, the 2-D models tend to predict increased spreading in the lateral and vertical dimensions in addition to higher maximum saturations.

[19] Alternatively, the ability of 2-D simulations to represent the saturation distributions simulated in the entire 3-D domain can be assessed by comparing saturation distribution spreading metrics calculated in 2-D and in 3-D. Statistics calculated for the ensemble of 3-D saturation distribution metrics are also given in Table 2. Mean metric values calculated in 3-D simulations are within 10–30% of metrics calculated in 2-D simulations and the 2-D metrics are slightly larger than the 3-D metrics. s_o^{\max} is the only metric that does not follow this trend. Figure 3 shows that s_o^{\max} for 2-D simulations are slightly lower than s_o^{\max} calculated for the entire 3-D domain. A paired t-test [Devore, 1995] showed that, in contrast to the 2-D versus “2-D in 3-D” comparison, the 2-D and 3-D mean s_o^{\max} values are equivalent at the 95% confidence level.

[20] The equivalence of s_o^{\max} in 2-D and 3-D, however, may be an artifact of the selected spill volume or source strength (release rate). Other investigators [e.g., Kueper and Gerhard, 1995] have demonstrated that saturation distribution metric values in 2-D simulations were sensitive to the release rate and spill volume. Therefore to assess the influence of these factors on the s_o^{\max} observation in this study, three realizations corresponding to the min, mean, and max s_o^{\max} values simulated in “2-D in 3-D” were selected from the set of 16. Two additional spill volumes (64L and 192L) were simulated in each realization by adjusting the duration of the spill (i.e., the release rate remained unchanged) and one additional release rate was simulated by doubling the source strength (0.64 L/d). Spill volume results are presented in Table 3 and release rate results are presented in Table 4. As shown in Table 3, an increase in spill volume resulted in an increase in the s_o^{\max} value, however the increase was observed in both 2-D and 3-D, suggesting that the approximate equivalence of s_o^{\max} in 2-D and 3-D is independent of spill volume. The spreading metrics reported in Table 3 also support the general observation that lateral and vertical spreading in 2-D will, on average, be greater than that simulated in 3-D, regardless of the spill volume. For the range of source strengths considered here, s_o^{\max} was insensitive to the release rate. Spreading metrics decreased slightly due primarily to larger initial

Table 3. Saturation Distribution Metrics for Three Alternative Realizations Subject to Three Different Spill Volumes^a

| Spill Volume | S_o^{\max} | | X_{cm} , m | | Z_{cm} , m | | σ_{xx}^2 , m ² | | σ_{zz}^2 , m ² | |
|--------------|--------------------|-------|--------------|-------|--------------|-------|----------------------------------|-------|----------------------------------|-------|
| | 2-D | 3-D | 2-D | 3-D | 2-D | 3-D | 2-D | 3-D | 2-D | 3-D |
| | <i>Minimum</i> | | | | | | | | | |
| 64L | 0.217 | 0.332 | 3.941 | 4.060 | 2.654 | 2.236 | 0.279 | 0.242 | 2.444 | 2.197 |
| 128L | 0.223 | 0.334 | 3.669 | 4.061 | 4.725 | 3.629 | 0.388 | 0.328 | 8.107 | 4.691 |
| 192L | 0.498 ^b | 0.425 | 3.390 | 4.041 | 6.170 | 4.631 | 1.191 | 0.422 | 10.571 | 6.958 |
| | <i>Mean</i> | | | | | | | | | |
| 64L | 0.305 | 0.396 | 3.752 | 3.877 | 2.379 | 2.038 | 0.366 | 0.259 | 1.608 | 1.291 |
| 128L | 0.354 | 0.397 | 3.758 | 3.865 | 3.579 | 3.164 | 1.115 | 0.464 | 2.882 | 2.613 |
| 192L | 0.356 | 0.397 | 3.828 | 3.851 | 4.779 | 4.103 | 1.563 | 0.607 | 5.833 | 4.482 |
| | <i>Maximum</i> | | | | | | | | | |
| 64L | 0.436 | 0.441 | 3.820 | 3.879 | 2.557 | 2.109 | 0.199 | 0.224 | 2.359 | 1.684 |
| 128L | 0.440 | 0.442 | 3.813 | 3.671 | 4.270 | 3.469 | 0.402 | 0.546 | 5.655 | 4.009 |
| 192L | 0.472 ^b | 0.442 | 3.765 | 3.571 | 5.558 | 4.515 | 0.747 | 0.697 | 8.611 | 6.263 |

^aSpill volumes were changed by increasing or decreasing the duration of the spill event. In all simulations the contaminant release rate in a given block remained unchanged. In all 2-D cases the spill volume is one-fourth the volume reported in the left-hand column.

^bThese saturations were larger than observed for other spill volumes due to pooling of NAPL on the bottom no-flow boundary.

water displacement and subsequently more entrapment (Table 4). Dimensionality did not appear to affect these results.

[21] As an alternative to the comparison of selected metric values, a $Q-Q$ plot can be used to compare the 2-D and 3-D saturation distributions directly. This plot is commonly found in the geostatistical literature [Goovaerts, 1997] and is based on the comparison of cumulative distribution functions. For this analysis a cumulative distribution function (CDF) of PCE saturations was generated for each 2-D and 3-D realization using all cells in the domain with a saturation greater than 0.0001. The 2-D and 3-D CDFs were averaged separately to generate two ensemble CDFs that were then used to generate the $Q-Q$ plot (Figure 5) (for details, see Goovaerts [1997]). This figure compares the average saturation for each CDF quantile. Much like a normality test, the degree to which values plot along the 1:1 line is an indication of the similarity in distributions. Examination of Figure 4 shows that the ensemble CDF in two and three dimensions is visually similar, with the 2-D CDF generally resulting in saturations 15–50% higher at the same quantile. This observation, when

combined with the results previously presented for the individual metrics, supports the premise that DNAPL infiltration and entrapment simulations conducted in 2-D domains will result in slightly higher estimates of NAPL saturations than simulations conducted in fully 3-D domains.

[22] In contrast to the spreading metrics discussed above, which quantify the spatial distribution of DNAPL saturation values in the domain, Lemke *et al.* [2004b] recently showed that long-term dissolution behavior can be significantly influenced by the distribution of mass between cells classified as pools and ganglia. This distribution of mass can be quantified by the GTP mass ratio defined in section 2. Figure 5 is a scatterplot of 3-D and “2-D in 3-D” versus 2-D GTP mass ratios for all 16 realizations considered in this study. From this figure, a positive trend in the simulated mass distribution is apparent. Despite several points that do not follow the general trend, there is a statistically significant (p -value = 0.0016) positive correlation ($\rho = 0.721$) between the 3-D and 2-D data (closed boxes) and the “2-D in 3-D” and 2-D data (open boxes, $\rho = 0.765$, p -value = 0.0002). In both the 3-D and “2-D in 3-D” comparisons, 75% of the data points fall above a 1:1 line,

Table 4. Saturation Distribution Metrics for Three Alternative Realizations Subject to Two Different Release Rates^a

| Release Rate, L/d | S_o^{\max} | | X_{cm} , m | | Z_{cm} , m | | σ_{xx}^2 , m ² | | σ_{zz}^2 , m ² | |
|-------------------|----------------|-------|--------------|-------|--------------|-------|----------------------------------|-------|----------------------------------|-------|
| | 2-D | 3-D | 2-D | 3-D | 2-D | 3-D | 2-D | 3-D | 2-D | 3-D |
| | <i>Minimum</i> | | | | | | | | | |
| 0.32 | 0.223 | 0.334 | 3.669 | 4.061 | 4.725 | 3.629 | 0.388 | 0.328 | 8.107 | 4.691 |
| 0.64 | 0.227 | 0.337 | 3.714 | 4.052 | 4.005 | 3.140 | 0.364 | 0.291 | 5.859 | 3.761 |
| | <i>Mean</i> | | | | | | | | | |
| 0.32 | 0.354 | 0.397 | 3.758 | 3.865 | 3.579 | 3.164 | 1.115 | 0.464 | 2.882 | 2.613 |
| 0.64 | 0.354 | 0.398 | 3.741 | 3.861 | 3.230 | 2.796 | 0.876 | 0.390 | 2.498 | 2.188 |
| | <i>Maximum</i> | | | | | | | | | |
| 0.32 | 0.440 | 0.442 | 3.813 | 3.671 | 4.270 | 3.469 | 0.402 | 0.546 | 5.655 | 4.009 |
| 0.64 | 0.441 | 0.444 | 3.803 | 3.740 | 3.726 | 3.026 | 0.331 | 0.447 | 4.330 | 3.177 |

^aIn all simulations, spill volume remained unchanged. In all 2-D cases the spill volume is one-fourth the volume reported in the left-hand column.

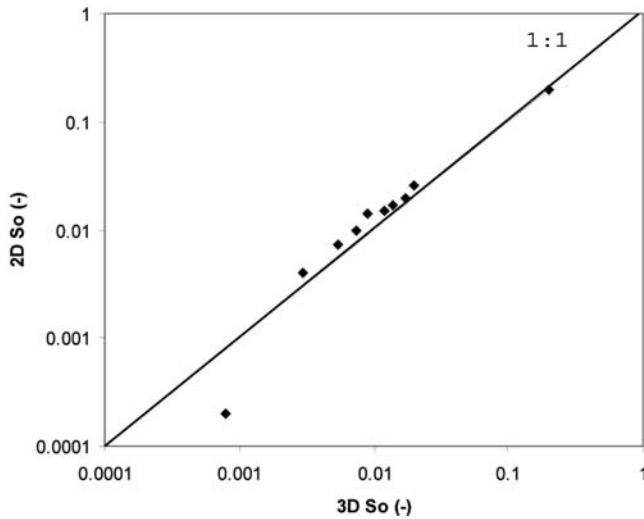


Figure 4. $Q-Q$ plot comparing saturation cumulative distribution functions generated using all contaminated cells ($s_o > 0.0001$) in 2-D and 3-D domains. A low value corresponds to the 10th percentile and may be an artifact of the large difference (~ 1 order of magnitude) in the number of cells with a quantifiable saturation in 2-D and 3-D domains.

indicating that the mass distributions simulated in 2-D generally resulted in higher levels of mass trapped in pools, which could affect predictions of source longevity [Anderson et al., 1992; Sale and McWhorter, 2001].

3.2. Realization Rank Calculations

[23] To compare the degree of variability in metric values across the ensemble of realizations simulated in two and three dimensions, each realization was rank ordered according to its metric value. Ranks of the 2-D simulations were plotted against ranks of the corresponding 2-D cross sections extracted from 3-D simulations and ranks of the corresponding 3-D simulations (Figure 6). Spearman rank correlation coefficients [Statistix, 1996] for all combinations are given in Table 5. The rank correlation coefficients for 2-D simulations and 2-D cross sections extracted from 3-D simulations (2-D in 3-D) are significant at or above the 95% confidence level for all metrics, indicating that 2-D cross sections representing average or extreme metric values tended to reproduce average or extreme metric values in the corresponding 2-D cross section in the 3-D domain. The same is true when comparing 2-D and 3-D simulations except for the σ_{xx}^2 metric (Figure 6e). The lower correlation of the metric between 2-D and 3-D simulations may result from greater variability in spreading in the x direction in 2-D simulations than in 3-D simulations. In fact, metric standard deviation for the 3-D simulations is smallest for all 5 of the metrics in Table 2. Thus evaluating behavior over the entire 3-D domain appears to have a smoothing effect on the metrics selected for analysis in this study.

3.3. Variability in the Horizontal Direction

[24] Performing DNAPL migration and entrapment simulations in 3-D gives the opportunity to investigate spreading behavior in different directions. One potential regulatory

compliance alternative to maximum contaminant levels (MCLs) is a regulatory threshold based on contaminant mass flux estimates through a down-gradient plane of compliance [Rao et al., 2002; Stroo et al., 2003]. The NAPL saturation distribution in the horizontal direction perpendicular to the direction of groundwater flow is very important to the determination of mass flux [Feenstra et al., 1996; Einarson and Mackay, 2001; Rao et al., 2002; Lemke et al., 2004b]. Typical 2-D models assume a nominal dimension in the direction perpendicular to flow [e.g., Abriola et al., 1992]. Hence upscaling 2-D simulations of source zone dissolution to 3-D is problematic. One logical approach is to assume that horizontal isotropy in permeability will lead to an isotropic source configuration (e.g., $\sigma_{xx}^2 = \sigma_{yy}^2$).

[25] To evaluate this hypothesis, the suite of 16 three-dimensional simulations was interrogated to determine if isotropic variability of permeability in the horizontal direction is associated with a symmetric source configuration. Substituting y for x in (4)–(6) facilitates the calculation of the center of mass in the y direction (Y_{cm}) and the second spatial moment about that center of mass (σ_{yy}^2). A scatterplot of σ_{xx}^2 versus σ_{yy}^2 for the 16 realizations is shown in Figure 7. It is apparent from this figure that there is no correlation between spreading in the x and y direction ($\rho = 0.311$). The mean spreading for the suite of realizations in each direction, however, is statistically identical at the 95% confidence level using a paired t-test. These results suggest that spreading in the x and y direction may be different for any realization, but the average spreading in each direction across an ensemble of realizations is expected to be the same.

[26] The variability among realizations observed in Figure 7 is possibly due to the release rate or extent (area) of the spill, which extends across approximately $1/2$ the horizontal integral scale of the permeability field. In a 2-D study investigating the influence of source dimensions on spreading, Kueper and Gerhard [1995] found that the

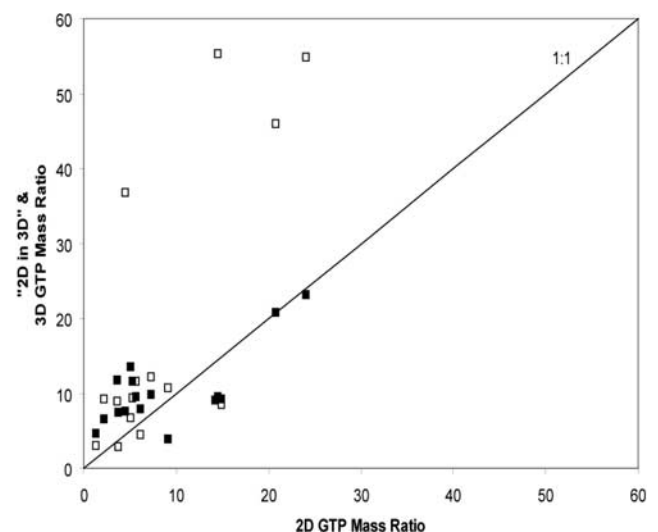


Figure 5. Scatterplot of 2-D versus “2-D in 3-D” (open boxes) and 3-D (closed boxes) ganglia-to-pool (GTP) mass ratios. Note that one “2-D in 3-D” realization had a GTP mass ratio = ∞ . This point is not shown.

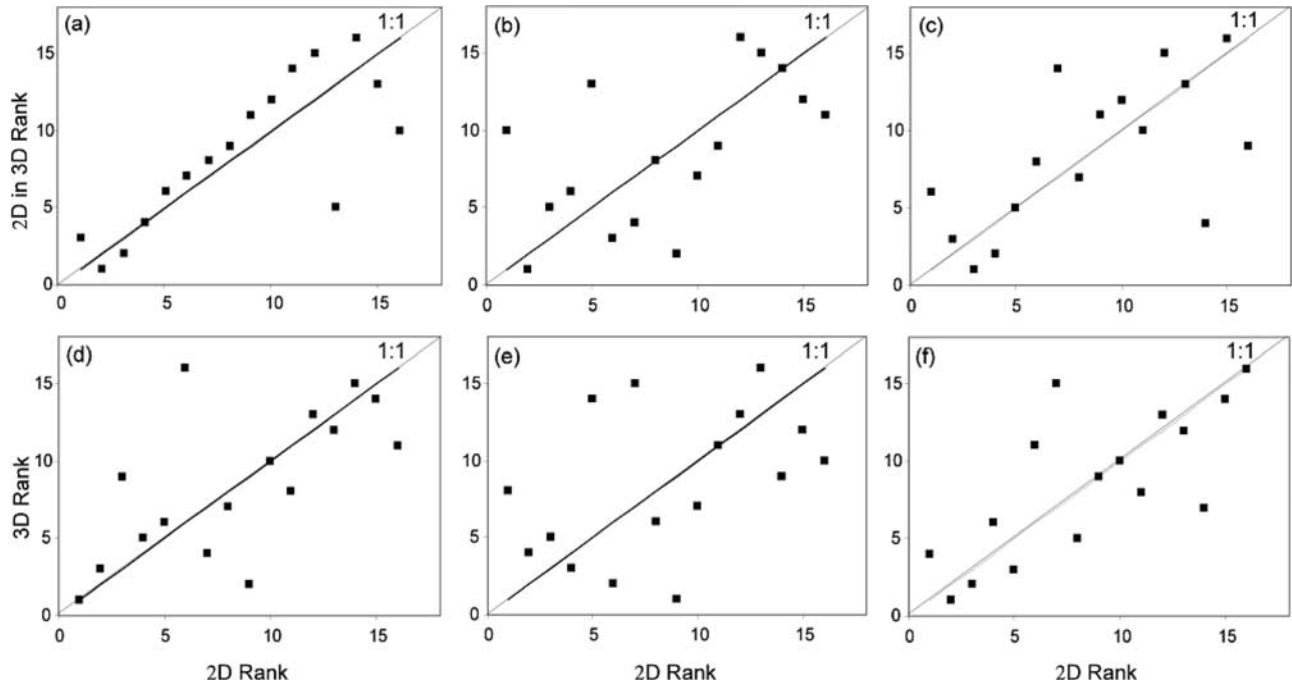


Figure 6. Scatterplots of realization ranks based on metric values: (a) 2-D versus “2-D in 3-D” s_o^{\max} , (b) 2-D versus “2-D in 3-D” σ_{xx}^2 , (c) 2-D versus “2-D in 3-D” σ_{zz}^2 , (d) 2-D versus 3-D s_o^{\max} , (e) 2-D versus 3-D σ_{xx}^2 , and (f) 2-D versus 3-D σ_{zz}^2 .

degree of lateral spreading was highly dependent on the permeability field near the spill release area for spills with dimensions less than the permeability field integral scale. In a separate numerical experiment, these authors also show that as the rate of release (source strength) increases both the degree of lateral spreading and the tortuosity of the infiltrating DNAPL path decrease. Hence the DNAPL mass distribution for any single realization as well as the average spreading over a suite of realizations is expected to become even more symmetric as the spill area or release rate increase. Note, however, for the higher release rate discussed in section 3.1 only a marginal increase ($\sim 4\%$) in the symmetry between σ_{xx}^2 and σ_{yy}^2 was observed (metric values not shown). Therefore while the results of this study show that the ensemble average 2-D spreading metric will provide a good approximation to this metric for a symmetric 3-D source zone, symmetric 3-D spreading for an individual realization is likely to be realized only at sites where the source zone area is larger than the integral scale or a release rate larger than those considered here can be assumed.

3.4. Influence of Increased $\sigma^2 \ln(K)$

[27] The simulations reported above were for a relatively homogeneous (low variance) porous medium. To explore the influence of increasing nonuniformity on the conclu-

sions of this study, additional simulations were performed with different permeability fields. Three 3-D permeability realizations (chosen based on min, mean, and max “2-D in 3-D” s_o^{\max} values) were transformed from a $\sigma^2 \ln(K) = 0.29$, which corresponded to the Oscada, MI aquifer, to a $\sigma^2 \ln(K) = 1.0$, corresponding to a moderately nonuniform aquifer. The center 2-D cross section was then extracted from the 3-D domain and 2-D and 3-D simulations were performed using UTCHEM. All simulation parameters, other than the permeability field, remained the same.

[28] Although it is difficult to calculate meaningful statistics with three realizations, the results of these simulations are consistent with most of the observations made using the 16 lower-variance permeability realizations. Comparison of the metrics calculated for the higher- and lower-variance realizations (Table 6) shows that the maximum saturation and horizontal spreading generally increase with variance, while the GTP mass ratio and the horizontal and vertical centers of mass decrease, regardless of dimensionality. Changes in vertical spreading due to an increase in the variance appear to be dependent on the realization, but not on the dimensionality. As with the original set of 16 realizations, the 2-D s_o^{\max} , σ_{xx}^2 , and σ_{zz}^2 metric values are generally larger and the GTP mass ratio is generally smaller than the “2-D in 3-D” simulation metric values and the

Table 5. Spearman Rank Correlation Coefficients

| | s_o^{\max} | σ_{xx}^2 | σ_{zz}^2 |
|--|--------------|-----------------|-----------------|
| 2-D versus 2-D in 3-D (significance level, %) ^a | 0.788 (99.5) | 0.576 (95) | 0.624 (98) |
| 2-D versus 3-D (significance level, %) ^a | 0.653 (98.5) | 0.447 (<95) | 0.738 (99.4) |

^aOne minus the significance level is the percent likelihood that the calculated correlation is due to chance.

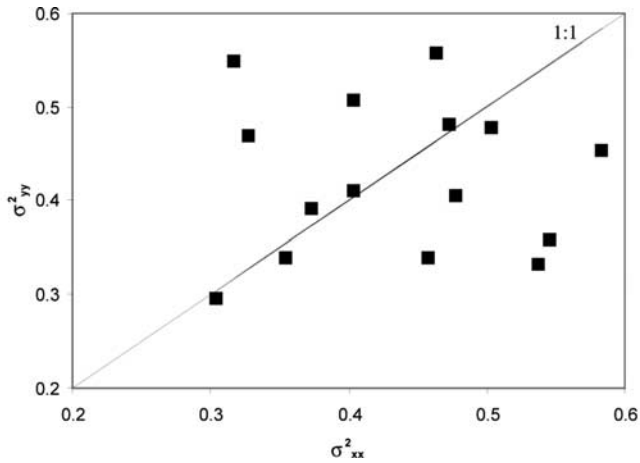


Figure 7. Scatterplot of σ_{yy}^2 versus σ_{xx}^2 metrics.

relative rank of the realization for each metric remains unchanged at the higher variance. Comparing the higher-variance 2-D and 3-D results shows that, as observed for the ensemble of 16 realizations, the s_o^{\max} metric values and GTP mass ratios are closely related (generally <20% difference). Spreading metrics, however, are more difficult to interpret. 2-D versus 3-D comparisons of lateral spreading are realization-dependent and only 2 out of the 3 selected realizations (MIN and MAX) result in 3-D vertical spreading that is smaller than 2-D. This behavior could be an artifact of the SGS routine used to generate the permeability field or could reflect the fact that these three realizations were selected based on maximum saturations without regard for spreading behavior. SGS routines tend to maximize the entropy in the simulated field [Deutsch and Journel, 1998] and as observed in Table 2 and Figure 3 spreading metrics were generally characterized by much greater variability. Thus

the conclusions of this study regarding 2-D and 3-D lateral spreading should be used with caution when considering aquifers characterized by a more highly nonuniform permeability field or a heterogeneous permeability field with discrete, multimodal populations of k values. As the degree of nonuniformity increases it may become necessary to perform migration and entrapment simulations in 3-D domains to capture the degree of lateral and vertical spreading.

4. Conclusions

[29] The influence of dimensionality on the development of realistic DNAPL source zone saturation distributions was investigated by conducting numerical simulations in 16 alternative realizations of a three dimensional, statistically homogeneous, nonuniform permeability field using the multiphase flow simulator, UTCHEM. This work appears to be the first to document use of the hysteretic entrapment model in UTCHEM, although coding corrections were required for its proper implementation.

[30] A reduction in dimensionality from 3-D to 2-D was shown to have a reasonably consistent impact on the predicted characteristics of the DNAPL source zone. Direct scaling of these metrics from 2-D to 3-D is not possible, however, based on the results of this study. 2-D simulations tended to have a 20–30% higher maximum NAPL saturation and increased spreading in the horizontal and vertical directions when compared to equivalent 2-D cross sections extracted from 3-D domains. The maximum saturations simulated in 2-D and the fully 3-D domains were shown to be statistically identical at the 95% confidence level. A comparison of GTP mass ratios for 2-D and 3-D simulations demonstrated that the simulated distribution of mass between pools and ganglia in 2-D was positively correlated to the mass distribution simulated in 3-D. Variability in 2-D and 3-D NAPL saturation distributions across realizations

Table 6. Statistics for Saturation Distribution Metrics in 2-D and 3-D Realizations With $\sigma^2 \ln(K) = 1.0^a$

| Metric | Simulation | Minimum | | Mean | | Maximum | |
|-----------------|-------------------------|-------------------|------------------|-------------------|------------------|-------------------|------------------|
| | | 0.29 ^b | 1.0 ^b | 0.29 ^b | 1.0 ^b | 0.29 ^b | 1.0 ^b |
| s_o^{\max} | 2-D | 0.223 | 0.521 | 0.354 | 0.508 | 0.440 | 0.602 |
| | 2-D in 3-D ^c | 0.134 | 0.268 | 0.275 | 0.464 | 0.442 | 0.584 |
| | 3-D ^d | 0.334 | 0.618 | 0.397 | 0.587 | 0.442 | 0.584 |
| X_{cm} | 2-D | 3.669 | 3.746 | 3.758 | 3.404 | 3.813 | 3.254 |
| | 2-D in 3-D | 4.222 | 3.989 | 3.533 | 2.879 | 3.531 | 3.458 |
| | 3-D | 4.060 | 4.191 | 3.865 | 3.379 | 3.671 | 3.488 |
| σ_{xx}^2 | 2-D | 0.388 | 0.479 | 1.115 | 0.952 | 0.402 | 0.868 |
| | 2-D in 3-D | 0.389 | 0.438 | 0.692 | 1.347 | 0.642 | 0.777 |
| | 3-D | 0.328 | 0.534 | 0.464 | 1.480 | 0.546 | 0.737 |
| Z_{cm} | 2-D | 4.725 | 5.744 | 3.575 | 2.925 | 4.270 | 4.110 |
| | 2-D in 3-D | 3.880 | 3.317 | 2.660 | 2.844 | 3.749 | 3.230 |
| | 3-D | 3.629 | 3.132 | 3.164 | 3.013 | 3.469 | 3.098 |
| σ_{zz}^2 | 2-D | 8.107 | 9.891 | 2.882 | 1.852 | 5.655 | 4.799 |
| | 2-D in 3-D | 5.385 | 3.448 | 1.971 | 2.005 | 4.371 | 3.713 |
| | 3-D | 4.691 | 2.805 | 2.613 | 2.893 | 4.009 | 2.839 |
| GTP | 2-D | 14.26 | 1.79 | 3.63 | 1.22 | 14.91 | 1.76 |
| | 2-D in 3-D | ∞ | 4.89 | 8.83 | 2.54 | 8.39 | 2.31 |
| | 3-D | 9.03 | 1.49 | 11.69 | 1.88 | 9.22 | 2.13 |

^aA GTP mass ratio = ∞ indicates that the maximum saturation is less than the maximum residual organic saturation in all cells in the domain.

^b $\sigma^2 \ln(K)$.

^cMetrics calculated for center 2-D x - z cross section in 3-D simulation.

^dMetrics calculated for entire 3-D domain.

was shown to be similar; indicating extreme behavior in the 3-D realization will often be mimicked in simulations conducted in 2-D slices extracted from the same 3-D realization. Horizontal isotropic variability did not result in a symmetric x - y saturation distribution for any individual 3-D realization. However, average spreading in the horizontal direction was symmetric for the 16 simulated realizations. This suggests that ensembles of 2-D realizations can be analyzed to infer average DNAPL infiltration and entrapment behavior along 2-D transects, irrespective of their orientation, when horizontal isotropy and bedding can be assumed.

[31] The observations reported above were also found to be valid for a small subset of realizations with an increased variance in the permeability field ($\sigma^2 \ln(K) = 1$). However, as the variance in the permeability field increased, lateral spreading of the DNAPL was enhanced in 3-D simulations to a greater extent than in 2-D simulations. This observation suggests that it may be necessary to perform 3-D simulations to capture the increased lateral spreading in highly variable formations.

[32] For statistically homogeneous, nonuniform permeability fields generated using SGS, the implications of this work are that DNAPL saturation distributions simulated in 2-D capture the essential characteristics, as quantified by the selected metrics, of a more realistic 3-D DNAPL saturation distribution. Hence for the analysis of DNAPL infiltration and entrapment behavior using the selected metrics, the more computationally efficient 2-D simulations can provide a good approximation to the fully 3-D simulation. However, caution must be used when considering highly nonuniform aquifers or aquifers that do not have horizontal bedding. Additional work is also required to explore whether equivalent migration and entrapment behavior simulated in 2-D and 3-D will result in equivalent mass recovery (dissolution) when simulated in 2-D and 3-D.

[33] **Acknowledgments.** This research was sponsored by the Strategic Environmental Research and Development Program (contract DACA72-00-C-0023). The content of this manuscript has not been subject to agency review and does not necessarily represent the views of the agency sponsor. We thank the anonymous reviewers and Associate Editor for their helpful comments on an earlier version of this manuscript.

References

- Abriola, L. M. (1989), Modeling multiphase migration of organic chemicals in groundwater systems—A review and assessment, *Environ. Health Perspect.*, **83**, 117–143.
- Abriola, L. M., K. Rathfelder, S. Yadav, and M. Maiza (1992), VALOR code version 1.0: A PC code for simulating subsurface immiscible contaminant transport, *Final Rep. EPRI TR-101018*, Electr. Power Res. Inst., Palo Alto, Calif.
- Abriola, L. M., C. D. Drummond, E. J. Hahn, K. F. Hayes, T. C. G. Kibbey, L. D. Lemke, K. D. Pennell, E. A. Petrouskis, C. A. Ramsburg, and K. M. Rathfelder (2005), A pilot-scale demonstration of surfactant-enhanced PCE solubilization at the Bachman Road site: 1. Site characterization and test design, *Environ. Sci. Technol.*, in press.
- Adeel, Z., J. W. Mercer, and C. R. Faust (2001), Models for describing multiphase flow and transport of contaminants, *Am. Soc. Civ. Eng. Manuals Rep. Eng. Pract.*, **100**, 1–39.
- Anderson, M. R., R. L. Johnson, and J. F. Pankow (1992), Dissolution of dense chlorinated solvents into groundwater: 3. Modeling contaminant plumes from fingers and pools of solvent, *Environ. Sci. Technol.*, **26**, 901–908.
- Bradford, S. A., L. M. Abriola, and K. M. Rathfelder (1998), Flow and entrapment of dense nonaqueous phase liquids in physically and chemically heterogeneous aquifer formations, *Adv. Water Resour.*, **22**, 117–132.
- Brooks, R. H., and A. T. Corey (1964), Hydraulic properties of porous media, *Hydrol. Pap. 3*, Colo. State Univ., Fort Collins, Colo.
- Brown, C. L., G. A. Pope, L. M. Abriola, and K. Sepehrmoori (1994), Simulation of surfactant-enhanced aquifer remediation, *Water Resour. Res.*, **30**, 2959–2977.
- Burdine, H. T. (1953), Relative permeability calculations from pore-size distribution data, *Trans. Soc. Pet. Eng. AIME*, **198**, 71–77.
- Dekker, T. J., and L. M. Abriola (2000), The influence of field-scale heterogeneity on the infiltration and entrapment of dense nonaqueous phase liquids in saturated formation, *J. Contam. Hydrol.*, **42**, 187–218.
- Delshad, M., G. A. Pope, and K. Sepehrmoori (1996), A compositional simulator for modeling surfactant enhanced aquifer remediation: 1. Formulation, *J. Contam. Hydrol.*, **23**, 303–327.
- Delshad, M., L. Yeh, and F. J. Holzmer (2000), Design of the surfactant flood at Camp Lejeune, in *Treating Dense Nonaqueous Phase Liquids (DNAPLs): Remediation of Chlorinated and Recalcitrant Compounds*, edited by G. B. Wickramanayake, A. R. Gavaskar, and N. Gupta, pp. 203–210, Batelle Press, Columbus, Ohio.
- Demond, A. H., K. Rathfelder, and L. M. Abriola (1996), Simulation of organic liquid flow in porous media using estimated and measured transport properties, *J. Contam. Hydrol.*, **22**, 223–239.
- Deutsch, C. V., and A. G. Journel (1998), *GSLIB Geostatistical Software Library and User's Guide*, 2nd ed., Oxford Univ. Press, New York.
- Devore, J. L. (1995), *Probability and Statistics for Engineering and the Sciences*, 4th ed., Wadsworth, Belmont, Calif.
- Drummond, C. D., L. D. Lemke, K. M. Rathfelder, E. J. Hahn, and L. M. Abriola (2000), Simulation of surfactant-enhanced PCE recovery at a pilot test field site, in *Treating Dense Nonaqueous Phase Liquids (DNAPLs): Remediation of Chlorinated and Recalcitrant Compounds*, edited by G. B. Wickramanayake, A. R. Gavaskar, and N. Gupta, pp. 77–84, Batelle Press, Columbus, Ohio.
- Edwards, M. G., M. Delshad, G. A. Pope, and K. Sepehrmoori (1999), A high-resolution method coupled with local grid refinement for three-dimensional aquifer remediation, *In Situ*, **23**, 333–377.
- Einarson, M. D., and D. M. Mackay (2001), Predicting impacts of ground water contamination, *Environ. Sci. Technol.*, **35**, 67A–73A.
- Essaid, H. I., and K. M. Hess (1993), Monte Carlo simulations of multiphase flow incorporating spatial variability of hydraulic properties, *Ground Water*, **31**, 123–134.
- Essaid, H. I., W. N. Herkelrath, and K. M. Hess (1993), Simulation of fluid distributions observed at a crude oil spill site incorporating hysteresis, oil entrapment, and spatial variability of hydraulic properties, *Water Resour. Res.*, **29**, 1753–1770.
- Faust, C. R., J. H. Guswa, and J. W. Mercer (1989), Simulation of three-dimensional flow of immiscible fluids within and below the unsaturated zone, *Water Resour. Res.*, **25**, 2449–2464.
- Feenstra, S., J. A. Cherry, and B. L. Parker (1996), Conceptual models for the behavior of nonaqueous phase liquids (DNAPLs) in the subsurface, in *Dense Chlorinated Solvents and Other DNAPLs in Groundwater*, edited by J. F. Pankow and J. A. Cherry, pp. 53–88, Waterloo Press, Portland, Ore.
- Glass, R. J., S. H. Conrad, and W. Peplinski (2000), Gravity-destabilized nonwetting phase invasion in macroheterogeneous porous media: Experimental observations of invasion dynamics and scale analysis, *Water Resour. Res.*, **36**, 3121–3137.
- Goovaerts, P. (1997), *Geostatistics for Natural Resources Evaluation*, Oxford Univ. Press, New York.
- Guarnaccia, I., and G. Pinder (1998), On the importance of dimensionality in the simulation of dense non-aqueous liquid migration in the subsurface, in *Soil and Aquifer Pollution Non-Aqueous Phase Liquids—Contamination and Reclamation*, edited by H. Rubin, N. Narkis, and J. Carberry, pp. 209–219, Springer, New York.
- Haverkamp, R., and J. Y. Parlange (1986), Predicting the water-retention curve from particle-size distributions: 1. Sandy soils without organic matter, *Soil Sci.*, **142**, 325–339.
- Imhoff, P. T., A. S. Mann, M. Mercer, and M. Fitzpatrick (2003), Scaling DNAPL migration from the laboratory to the field, *J. Contam. Hydrol.*, **1822**, 1–20.
- Jin, M., G. W. Butler, R. E. Jackson, P. E. Mariner, J. F. Pickens, G. A. Pope, C. L. Brown, and D. C. McKinney (1997), Sensitivity models and design protocol for partitioning tracer tests in alluvial aquifers, *Ground Water*, **35**, 964–972.
- Journel, A. G., and C. J. Huijbregts (1978), *Mining Geostatistics*, Elsevier, New York.
- Kueper, B. H., and E. O. Frind (1991), Two-phase flow in heterogeneous porous media: 2. Model application, *Water Resour. Res.*, **27**, 1059–1070.

- Kueper, B. H., and J. I. Gerhard (1995), Variability of point source infiltration rates for two-phase flow in heterogeneous porous media, *Water Resour. Res.*, *31*, 2971–2980.
- Kueper, B. H., D. Redman, R. C. Starr, S. Reitsma, and M. Mah (1993), A field experiment to study the behavior of tetrachloroethylene below the water table: Spatial distribution of residual and pooled DNAPL, *Ground Water*, *31*, 756–766.
- Lemke, L. D., and L. M. Abriola (2003), Predicting DNAPL entrapment and recovery: The influence of hydraulic property correlation, *Stochastic Environ. Res. Risk Assess.*, *17*, 408–418, doi:10.1007/S00477-003-0162-4.
- Lemke, L. D., L. M. Abriola, and P. Goovaerts (2004a), Dense nonaqueous phase liquid (DNAPL) source zone characterization: Influence of hydraulic property correlation on predictions of DNAPL infiltration and entrapment, *Water Resour. Res.*, *40*, W01511, doi:10.1029/2003WR001980.
- Lemke, L. D., L. M. Abriola, and J. R. Lang (2004b), Influence of hydraulic property correlation on predicted dense nonaqueous phase liquid source zone architecture, mass recovery and contaminant flux, *Water Resour. Res.*, *40*, W12417, doi:10.1029/2004WR003061.
- Leverett, M. C. (1941), Capillary behavior in porous solids, *Trans. Am. Inst. Min. Metall. Eng. Pet. Eng. Div.*, *142*, 152–169.
- Miller, C. T., G. Christakos, P. T. Imhoff, J. F. McBride, J. A. Pedit, and J. A. Trangenstein (1998), Multiphase flow and transport modeling in heterogeneous porous media: Challenges and approaches, *Adv. Water Resour.*, *21*, 77–120.
- Ouyang, Y., J. S. Cho, and R. S. Mansell (2002), Simulated formation and flow of microemulsions during surfactant flushing of contaminated soil, *Water Res.*, *36*, 33–40.
- Panday, S., Y. S. Wu, P. S. Huyakorn, and E. P. Springer (1994), A three-dimensional multiphase flow model for assessing NAPL contamination in porous and fractured media: 2. Porous medium simulation examples, *J. Contam. Hydrol.*, *16*, 131–156.
- Parker, J. C., and R. J. Lenhard (1987), A model for hysteretic constitutive relations governing multiphase flow: 1. Saturation-pressure relations, *Water Resour. Res.*, *23*, 2187–2196.
- Pouslen, M. M., and B. H. Kueper (1992), A field experiment to study the behavior of tetrachloroethylene in unsaturated porous media, *Environ. Sci. Technol.*, *26*, 889–895.
- Rao, P. S., J. W. Jawitz, G. C. Enfield, R. W. Falta, M. D. Annable, and A. L. Wood (2002), Technology integration for contaminated site remediation: Clean-up goals and performance criteria, *IAHS Publ.*, *275*, 571–578.
- Rathfelder, K., and L. M. Abriola (1998), The influence of capillarity in numerical modeling of organic liquid redistribution in two-phase systems, *Adv. Water Resour.*, *21*, 159–170.
- Rathfelder, K., L. M. Abriola, M. A. Singletary, and K. D. Pennell (2000), The influence of interfacial tension reduction on organic liquid migrations: Numerical and experimental comparisons, *IAHS Publ.*, *265*, 439–447.
- Rathfelder, K. M., L. M. Abriola, M. A. Singletary, and K. D. Pennell (2003), Influence of surfactant-facilitated interfacial tension reduction on chlorinated solvent migration in porous media: Observations and numerical simulations, *J. Contam. Hydrol.*, *64*, 227–252.
- Roeder, E., and R. W. Falta (2001), Modeling unstable alcohol flooding of DNAPL-contaminated columns, *Adv. Water Resour.*, *24*, 803–819.
- Sale, T. C., and D. B. McWhorter (2001), Steady state mass transfer from single-component dense nonaqueous phase liquids in uniform flow fields, *Water Resour. Res.*, *37*, 393–404.
- Statistix (1996), *Statistix for Windows User's Manual*, Analytical Software, Tallahassee, Fla.
- Stroo, H. F., M. Unger, C. H. Ward, M. C. Kavanaugh, C. Vogel, A. Leeson, J. A. Marqusee, and B. P. Smith (2003), Remediating chlorinated solvent source zones, *Environ. Sci. Technol.*, *37*, 224A–230A.
- University of Texas Chemical Compositional Simulator (UTCHEM) (2000), *Version 9.0 Technical Documentation*, Cent. for Pet. and Geosyst. Eng. Univ. of Texas, Austin, Tex.
- Whittaker, J., G. Teutsch, and P. Grathwohl (2000), DNAPL spill and plume migration in a naturally heterogeneous aquifer analogue, *IAHS Publ.*, *265*, 455–460.
- Wu, W.-J., M. Delshad, T. Oolman, and G. A. Pope (2000), Remedial options for creosote-contaminated sites, *Ground Water Monit. Remediation*, *20*, 78–86.
- Young, C. M., R. E. Jackson, M. Jin, J. T. Londergan, P. E. Mariner, G. A. Pope, F. J. Anderson, and T. Houk (1999), Characterization of a TCE DNAPL zone in alluvium by partitioning tracers, *Ground Water Monit. Remediation*, *19*, 84–94.

L. M. Abriola, Department of Civil and Environmental Engineering, 105 Anderson Hall, Tufts University, Medford, MA 02155, USA. (linda.abriola@tufts.edu)

J. A. Christ, Environmental and Water Resources Engineering Program, Room 116, EWRE Building, University of Michigan, 1351 Beale Avenue, Ann Arbor, MI 48109-2125, USA. (christj@umich.edu)

L. D. Lemke, Environmental Sciences Program, Department of Geology, Wayne State University, 0224 Old Main, Detroit, MI 48202, USA. (ldlemke@wayne.edu)